Compact 3-D-Printed 4 × 4 Butler Matrix Based on Low-Cost and Curing-Free Additive Manufacturing

Valentina Palazzi, *Member, IEEE*, Arianna Cicioni, Federico Alimenti, *Senior Member, IEEE*, Paolo Mezzanotte, *Member, IEEE*, Manos M. Tentzeris, *Fellow, IEEE*, and Luca Roselli, *Fellow, IEEE*

***Abstract*— This letter presents a 4 × 4 Butler matrix realized using stereolithography 3-D printing technology and liquid metal filling. The matrix is in coaxial technology and relies on circular branch lines and curved 50 Ω lines. Input and output ports are aligned and placed on the same plane, while branch lines are organized using all three dimensions to minimize the length of the connecting lines. A prototype, designed at an operating frequency of 12 GHz, is manufactured and tested, showing a footprint of only 1.7 × 1.3 λ_0^2. A good agreement between simulated and measured transmission coefficients is observed regardless of the selected input port. These encouraging results open the door to the realization of compact low-cost and high-performing RF beam-steering networks in coaxial technology, based on curing-free additive manufacturing processes.**

***Index Terms*— 3-D printing, additive manufacturing, Butler matrix, liquid metal, microfluidics, stereolithography.**

I. Introduction

3D PRINTING is an emerging approach to create complex RF circuits not feasible with standard subtracting technologies [1].

Among the solutions enabled by 3-D printing, there are unconventional antenna topologies [2], [3], innovative packaging solutions [4], [5], and RF crossovers [6]. In planar circuits, crossovers can be realized either using 0-dB branch lines, which are cumbersome and narrowband, or resorting to via signals and multilayer technologies, which are expensive. On the other hand, the third dimension can be used to overcome the limitations experienced by planar circuits, by allowing lines to lie on different portions of the space [6].

3-D printing can also be used to realize RF components by means of unconventional waveguide structures. Among them, coaxial technology has attracted significant attention [7]–[9]. In some contexts, it is preferred to microstrip technology for its higher immunity to interference, no air radiation, and lower dispersion. However, realizing coaxial RF components with variable line impedances is generally inconvenient with traditional manufacturing technologies. High-performing rectangular coaxial lines, based on sequential microfabrication processes, have been reported in [10]–[12]. These technologies, though, require the manufacturing of multilayer circuits. A 3-D-printed rectangular coaxial cable has been reported in [9], where the 3-D-printed dielectric is metalized via electroless plating. This approach leads to low-loss lines (the coaxial dielectric is just air), but holes must be made on the external conductor to enable electroplating of the internal surface, and quarter-wave short-circuited stubs must be used to support the inner conductor, leading to cumbersome components.

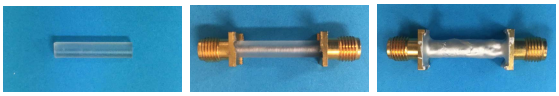

(a) (b) (c)

Fig. 1. Fabrication steps of additively manufactured coaxial line. (a) 3-D-printed dielectric, (b) prototype before colloidal silver deposition, and (c) complete prototype.

This letter presents a compact 4 × 4 Butler matrix in coaxial technology. A previous version of the matrix, with some preliminary results, was presented in [13], where, however, all 90° hybrid couplers were realized on the same plane. Here, not only the lines but also the hybrids are spatially arranged in an optimized configuration using all three dimensions to minimize the length of the connecting lines (the line length between each input and output port is reduced by 1.3 mm, with a reduction in the average insertion loss of 0.5 dB at the design frequency), and combining equally spaced parallel input and output ports with a compact layout. Furthermore, the outer conductor of the coaxial structure, which was realized using silver nanoparticle ink in [13], is here replaced by colloidal silver to remove any curing steps.

II. Manufacturing Technology

The process steps to realize coaxial lines are summarized in Fig. 1. First, the dielectric scaffolding is 3-D printed [see Fig. 1(a)]. The structure is oriented so that most of the channels are nearly perpendicular to the printing plate to avoid clogging. The channel diameter is adjusted at the design stage to precompensate systematic errors of the 3-D printing process [13]. Then, every channel is filled with a liquid metal alloy at room temperature. In the case of multiport circuits, all channel ends but one are closed with a sticky removable resin, and the ink is inserted with a syringe pump [14]. After the channel filling, the sub-miniature version A (SMA) connectors are attached to the prototype with a dielectric glue (liquid metal is sealed), as shown in Fig. 1(b). 50 Ω SMA end-launch female connectors with outside 0.76-mm center pins are used. Every pin is inserted in the corresponding channel of the

Manuscript received November 7, 2020; accepted November 25, 2020. Date of publication December 14, 2020; date of current version February 11, 2021. This work was supported by the Air Force Research Laboratory and the NSF-EFRI. The work was performed in part at the Georgia Tech Institute for Electronics and Nanotechnology, a member of the National Nanotechnology Coordinated Infrastructure (NNCI), which is supported by the National Science Foundation (Grant ECCS-1542174). *(Corresponding author: Valentina Palazzi.)*

Valentina Palazzi, Arianna Cicioni, Federico Alimenti, Paolo Mezzanotte, and Luca Roselli are with the Department of Engineering, University of Perugia, 06123 Perugia, Italy (e-mail: palazzi.valentina.89@gmail.com).

Manos M. Tentzeris is with the School of Electrical and Computer Engineering, Georgia Institute of Technology, Atlanta, GA 30332 USA.

Color versions of one or more figures in this letter are available at https://doi.org/10.1109/LMWC.2020.3041569.

Digital Object Identifier 10.1109/LMWC.2020.3041569

dielectric scaffolding to be in touch with the liquid metal (the amount of liquid metal is fine-tuned to guarantee low contact resistance). Finally, colloidal silver paste is applied to the exterior of the dielectric [see Fig. 1(c)], to both manufacture the outer conductor and to ensure the electrical connection of the circuit with the ground of SMA connectors. As the field is confined within the dielectric, the thickness variability in the paste has no impact on propagation. Alternative curing-free metallization techniques can be also used, such as sputtering deposition and electroless plating [8].

The characteristic impedance Z_c of a coaxial line depends on the ratio of the radius of the inner conductor r_1 to the radius of the outer conductor r_2 (corresponding to the inner and outer radii of the dielectric scaffolding) as follows:

$$Z_c = \frac{\eta}{2\pi} \ln\left(\frac{r_2}{r_1}\right) \tag{1}$$

where $\eta = (\mu/\epsilon)^{1/2}$ is the intrinsic impedance of the dielectric medium, and μ and ϵ are its complex permeability and permittivity, respectively. With the proposed fabrication process, r_1 can be readily changed by modifying the radius of the inner channel of the dielectric scaffolding, thereby making it possible to realize complex coaxial components with variable line impedances, with a few simple steps.

To fabricate proof-of-concept prototypes, the Form2 3-D printer by Formlabs is utilized [15]. The adopted printer is of low cost, and relies on stereolithography, a 3-D printing technique in which a photo-reactive liquid resin is UV cured by a laser beam. The maximum resolution for the printer is 25 μm. The adopted resin is the Clear material V4 [16], which has a permittivity of 2.7 and a loss tangent of 0.03 at 12 GHz [13]. This material is transparent, which allows for visual inspection of the metal filling procedure. Lower-loss photo-reactive resins are also available on the market, as shown in [8].

The metal used for the inner conductor is a eutectic gallium indium (EGaIn) alloy by Sigma Aldrich [17], with a conductivity of 4.3×10^6 S/m. This material is liquid at room temperature, and it is pumped into the channels using a syringe.

Finally, the outer conductor is realized with the Pelco Colloidal Silver by TedPella [18]. This paste is applied with a brush, solidifies at room temperature in 16 h/20 h, has high adhesion and a conductivity of about 10^6 S/m. This way, curing steps can be avoided, thereby reducing the risks of dielectric deformation (the clear material has a heat deflection temperature of about 70 °C), and of EGaIn reflow and leakage out of the channels due to thermal expansion.

III. Circuit Design

The 4×4 Butler matrix in this work is based on standard circuit blocks: four circular branch-line couplers in coaxial technology (the shape of the coupler is chosen to get the largest spacing among the branches) [19], two phase shifters and two crossovers, made using 50 Ω curved pieces of coaxial lines.

The layout of the matrix, designed at 12 GHz with full-wave simulations (CAD CST Microwave Studio), is shown in Fig. 2. Both input (P1–P4) and output (P5–P8) ports of the network are aligned, lay on the same plane, and are matched to 50 Ω. The ports are evenly spaced by about 9.8 mm, which is the minimum distance required by SMA connectors. The distance among ports, however, can be modified based on the requirements of the circuit blocks connected to the matrix.

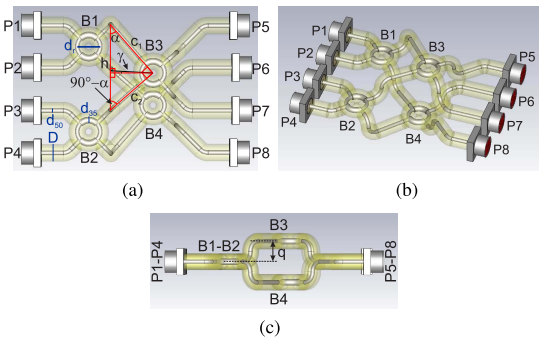

Fig. 2. Layout of the 4×4 Butler matrix: (a) top view, (b) perspective, and (c) side view. Main circuit parameters: $D = 4$ mm, $d_{50} = 1$ mm, $d_{35} = 1.55$ mm, $d_r = 5.3$ mm, $h = 19.6$ mm, $c_1 = 14.77$ mm, $c_2 = 12.88$ mm, $q = 5$ mm, $\alpha = 42.85°$, and $\gamma = 2.15°$.

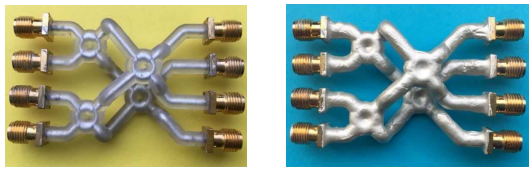

Fig. 3. Photographs of the fabricated prototype: (a) before colloidal silver deposition and (b) complete prototype.

The four 90° hybrids are labeled as B1, B2, B3, and B4 in Fig. 2. B1 and B2 are placed on the same plane. B3 and B4, instead, are placed one on a parallel plane above and the other on a parallel plane below the plane of the ports, respectively, to minimize the length of the two crossovers. The four output lines coming out of B3 and B4 have the same length (equal to 18 mm).

The design of the 45° phase shifters is based on the highlighted red triangle in Fig. 2(a). Every couple of lines connected to each branch line forms a 90° angle. Therefore, the triangle highlighted in Fig. 2(a) is a right triangle. To guarantee that the signal on the path c_1 is phase-shifted by 45° more than the signal on the path c_2, these path lengths must satisfy the following relationship:

$$c_1 = c_2 + \lambda_g/8 \tag{2}$$

where λ_g is the guided wavelength at the design frequency, and $\lambda_g/8$ is equal to 1.89 mm at 12 GHz. The hypotenuse h is known and fixed (determined by the distance among the input ports), therefore, c_1 and c_2 can be found as follows:

$$h = \sqrt{c_1^2 + c_2^2} = \sqrt{(c_2 + \lambda_g/8)^2 + c_2^2}. \tag{3}$$

Finally, the bending angle α is found as follows:

$$\alpha = \arcsin\left(\frac{c_2}{h}\right) = 42.85°. \tag{4}$$

Since α is different from 45°, the branch line B3 is rotated with respect to B1 and B2 by an angle γ defined as

$$\gamma = 45° - \alpha = 2.15° \tag{5}$$

which is compensated by the bending angles at the output lines, so that all output ports are parallel to each other.

The final prototype can be enclosed in brick with volume $43.3 \times 33.2 \times 17$ mm^3, including input and output lines.

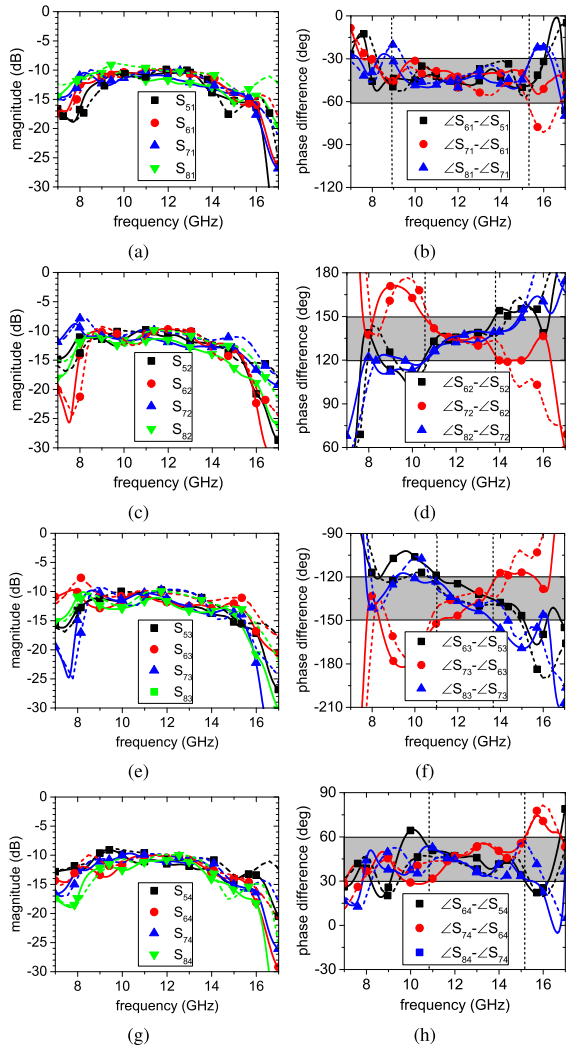

Fig. 4. Simulated (dashed line) and measured (solid line) transmission coefficients of the Butler matrix: (a), (c), (e), and (g) magnitude and (b), (d), (f), and (h) phase difference.

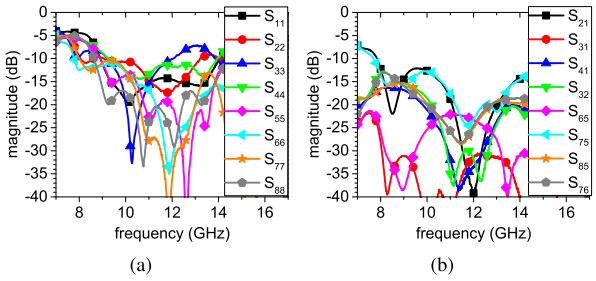

Fig. 5. Measured S-parameters of the Butler matrix: (a) return loss and (b) isolation.

The .stl file of the dielectric scaffolding is imported in the Preform CAD [20] utilized by the printer.

IV. Experimental Results

Fig. 3 shows the prototype fabricated with the process described in Section II. The S-parameters of the matrix are measured with a vector network analyzer. The magnitude and phase difference between the transmission coefficients are shown in Fig. 4. A good agreement between simulations and measurements is observed. The measured average magnitude of the transmission coefficients at 12 GHz is −11 dB for ports 1, 2, and 4, and −11.5 dB for port 3 (due to its higher return loss), while the simulated average value is −10 dB for all ports. The high loss of the circuit is mostly due to the 3-D-printed dielectric. Magnitude discrepancies between simulations and measurements can be due to imperfect channel filling and metal coating, and variations in the channel dimensions.

Although narrowband components are used, the adoption of nondispersive transmission lines allows the matrix to operate on broadband. The band corresponding to a phase error lower than ±15°, see the gray-shaded regions in Fig. 4, is 11–13.6 GHz. The bandwidth is mainly limited by port 3, where the highest fabrication tolerances are observed. Within this band, the magnitude difference among the transmission coefficients of the matrix is lower than 2 dB, the measured return loss is better than −10 dB for all ports except for port 3, where a peak value of −7.2 dB is observed, and isolation is better than −16 dB, as shown in Fig. 5.

In Table I, the presented circuit topology is compared with previous 3-D printed and single-layer 4 × 4 Butler matrices. The proposed matrix has a smaller footprint than state-of-the-art solutions. In [22] compactness is achieved adopting a high-permittivity substrate, at the expense of using a different substrate for the antennas. With the proposed solution, both the feed network and the antennas can be realized with the same material. Additionally, although the matrix is not optimized for broadband performance, its operating bandwidth is superior to microstrip solutions, due to the nondispersive nature of coaxial technology, and the absence of 0-dB branch lines.

TABLE I
Comparison With the State of the Art

ref.	tech.	freq. (GHz)	ϵ_r	volume (λ_0^3)	mag. err. (dB)	phase err. (deg.)
this work	3D prin.	11 − 13.6	2.7	$1.7\times1.3\times0.56$	2	15
[13]	3D prin.	12	2.7	$1.8\times2.1\times0.65$	2†	5†
[21]	s. layer	6	2.2	$3.7\times1.5\times0.02$	0.8	6
[22]	s. layer	28	6.2	$1.7\times1.8\times0.02$	4.7*	16*
[23]	s. layer	27.5−28.3	2.2	$2.8\times3\times0.02$	/	14.5*

"3D prin." stands for 3D printing, "s. layer" stands for single layer. ∗ Value from simulation results. † Value from partial results.

V. Conclusion

A compact Butler matrix, based on curing-free and low-cost additive manufacturing, has been designed and tested. The fabrication process has been presented in detail and a proof-of-concept prototype, working at 12 GHz, has been characterized. The good agreement between simulations and measurements testifies that the accuracy of the proposed process is adequate for circuit fabrication up to at least Ku band that can be further extended using newly reported lower-loss 3-D printable materials. In the frequency range 11–13.6 GHz, magnitude and phase errors lower than 2 dB and 15° have been observed, which shows the potential of the proposed approach to realize low-cost broadband beam-steering networks. In future works, the building blocks of the matrix can be optimized to further improve its performance (see, for instance, [24]).

REFERENCES

[1] R. Bahr, B. Tehrani, and M. M. Tentzeris, "Exploring 3-D printing for new applications: Novel inkjet- and 3-D printed millimeter-wave components, interconnects, and systems," *IEEE Microw. Mag.*, vol. 19, no. 1, pp. 57–66, Jan. 2018.

[2] J. S. Silva, M. Garcia-Vigueras, T. Debogovic, J. R. Costa, C. A. Fernandes, and J. R. Mosig, "Stereolithography-based antennas for satellite communications in Ka-band," *Proc. IEEE*, vol. 105, no. 4, pp. 655–667, Apr. 2017.

[3] R. A. Bahr, Y. Fang, W. Su, B. Tehrani, V. Palazzi, and M. M. Tentzeris, "Novel uniquely 3D printed intricate Voronoi and fractal 3D antennas," in *IEEE MTT-S Int. Microw. Symp. Dig.*, Honolulu, HI, USA, Jun. 2017, pp. 1–4.

[4] X. He, B. K. Tehrani, R. Bahr, W. Su, and M. M. Tentzeris, "Additively manufactured mm-wave multichip modules with fully printed 'Smart' encapsulation structures," *IEEE Trans. Microw. Theory Techn.*, vol. 68, no. 7, pp. 2716–2724, Jul. 2020.

[5] M. T. Craton, J. D. Albrecht, P. Chahal, and J. Papapolymerou, "A chip-first approach to millimeter-wave circuit packaging," *IEEE Microw. Wireless Compon. Lett.*, vol. 29, no. 2, pp. 116–118, Feb. 2019.

[6] V. Palazzi *et al.*, "3-D-printing-based selective-ink-deposition technique enabling complex antenna and RF structures for 5G applications up to 6 GHz," *IEEE Trans. Compon., Packag., Manuf. Technol.*, vol. 9, no. 7, pp. 1434–1447, Jul. 2019.

[7] V. Gjokaj and P. Chahal, "3D printed hybrid rigid-flex coaxial-like transmission line structures," in *Proc. IEEE Int. Symp. Antennas Propag. USNC/URSI Nat. Radio Sci. Meeting*, Boston, MA, USA, Jul. 2018, pp. 1425–1426.

[8] J. Shen, D. P. Parekh, M. D. Dickey, and D. S. Ricketts, "3D printed coaxial transmission line using low loss dielectric and liquid metal conductor," in *IEEE MTT-S Int. Microw. Symp. Dig.*, Philadelphia, PA, USA, Jun. 2018, pp. 59–62.

[9] J. Li *et al.*, "A full X-band fully 3-D printed E-plane rectangular-coax-to-waveguide transition," in *IEEE MTT-S Int. Microw. Symp. Dig.*, Boston, MA, USA, Jun. 2019, pp. 1209–1212.

[10] D. Filipovic *et al.*, "Modeling, design, fabrication, and performance of rectangular μ-coaxial lines and components," in *IEEE MTT-S Int. Microw. Symp. Dig.*, San Francisco, CA, USA, Jun. 2006, pp. 1393–1396.

[11] M. J. Lancaster, J. Zhou, M. Ke, Y. Wang, and K. Jiang, "Design and high performance of a micromachined K-band rectangular coaxial cable," *IEEE Trans. Microw. Theory Techn.*, vol. 55, no. 7, pp. 1548–1553, Jul. 2007.

[12] J. M. Oliver, H. Kazemi, J.-M. Rollin, D. Sherrer, S. Huettner, and S. Raman, "Compact, low-loss, micromachined rectangular coaxial millimeter-wave power combining networks," in *IEEE MTT-S Int. Microw. Symp. Dig.*, Seattle, WA, USA, Jun. 2013, pp. 1–4.

[13] V. Palazzi, P. Mezzanotte, F. Alimenti, M. Tentzeris, and L. Roselli, "Microfluidics-based 3D-printed 4×4 butler matrix in coaxial technology for applications up to K band," in *IEEE MTT-S Int. Microw. Symp. Dig.*, Boston, MA, USA, Jun. 2019, pp. 1371–1374.

[14] W. Su, S. A. Nauroze, B. Ryan, and M. M. Tentzeris, "Novel 3D printed liquid-metal-alloy microfluidics-based zigzag and helical antennas for origami reconfigurable antenna 'trees,'" in *IEEE MTT-S Int. Microw. Symp. Dig.*, Honolulu, HI, USA, Jun. 2017, pp. 1579–1582.

[15] Formlabs. *Form 2*. Accessed: Nov. 27, 2020. [Online]. Available: https://formlabs.com/3d-printers/form-2/

[16] Formlabs. (Jan. 2019). *Materials Data Sheet Photopolymer Resin for Form 1+ and Form 2*. Accessed: Nov. 27, 2020. [Online]. Available: https://archive-media.formlabs.com/upload/XL-DataSheet.pdf

[17] S. Aldrich. *Gallium–Indium Eutectic (495425)*. Accessed: Nov. 27, 2020. [Online]. Available: https://www.sigmaaldrich.com/catalog/product/aldrich/495425?lang=it&region=IT

[18] Ted Pella Inc. *Pelco Colloidal Silver Product Numbers. 16031, 16034*. Accessed: Nov. 27, 2020. [Online]. Available: https://www.tedpella.com/technote_html/16031%2034%20TN.pdf

[19] P. Meaney, "A novel branch-line coupler design for millimeter-wave applications," in *Proc. IEEE Int. Dig. Microw. Symp.*, Dallas, TX, USA, May 1990, pp. 585–588.

[20] Formlabs. *Formlabs Software 3D Printing Setup, Management, and Monitoring Made Simple*. Accessed: Nov. 27, 2020. [Online]. Available: https://formlabs.com/software/#preform

[21] H. Ren, B. Arigong, M. Zhou, J. Ding, and H. Zhang, "A novel design of 4×4 butler matrix with relatively flexible phase differences," *IEEE Antennas Wireless Propag. Lett.*, vol. 15, pp. 1277–1280, 2016.

[22] S. Kim, S. Yoon, Y. Lee, and H. Shin, "A miniaturized butler matrix based switched beamforming antenna system in a two-layer hybrid stackup substrate for 5G applications," *Electronics*, vol. 8, no. 11, p. 1232, Oct. 2019.

[23] S. Trinh-Van, J. M. Lee, Y. Yang, K.-Y. Lee, and K. C. Hwang, "A sidelobe-reduced, four-beam array antenna fed by a modified 4×4 butler matrix for 5G applications," *IEEE Trans. Antennas Propag.*, vol. 67, no. 7, pp. 4528–4536, Jul. 2019.

[24] Y. Wu, J. Shen, and Y. Liu, "Comments on 'quasi-arbitrary phase-difference hybrid coupler,'" *IEEE Trans. Microw. Theory Techn.*, vol. 61, no. 4, pp. 1725–1727, Apr. 2013.